NOVA
SCIENCE PUBLISHERS, INC.

THE TELLURIC FIELD INDUCED BY TIDAL MOTION: A REVIEW OF THE PORTUGUESE EXPERIENCE

Fernando A. Monteiro Santos
Rita Nolasco
Martinho Marta-Almeida
António Soares
Ivo Bernardo
Rafael Luzio
Jesus Dubert
João M. Dias

In: "Sea Level Rise, Coastal Engineering, Shorelines and Tides"
Editor: Linda L. Wright
ISBN: 978-1-61728-655-1 2011

400 Oser Avenue, Suite 1600
Hauppauge, N. Y. 11788-3619
Phone (631) 231-7269
Fax (631) 231-8175
E-mail: main@novapublishers.com
http://www.novapublishers.com

In: Sea Level Rise, Coastal Engineering, Shorelines and Tides ISBN: 978-1-61728-655-1
Editor: Linda L. Wright, pp. 205-234

Chapter 10

THE TELLURIC FIELD INDUCED BY TIDAL MOTION: A REVIEW OF THE PORTUGUESE EXPERIENCE

Fernando A. Monteiro Santos*[*,1], Rita Nolasco[2], Martinho Marta-Almeida[2], António Soares[1], Ivo Bernardo[1], Rafael Luzio[1], Jesus Dubert[3] and João M. Dias[3]

[1]Instituto Don Luíz-Laboratório Associado,
Universidade de Lisboa,Campo Grande, Lisboa, Portugal
[2]CESAM, Universidade de Aveiro, Portugal.
[3]CESAM, Departamento de Física, Universidade de Aveiro, Portugal

Abstract

Electromagnetic fluctuations in the ocean have external sources like ionospheric–magnetospheric current systems, and purely internal oceanic sources associated with interaction between water velocity fields and the geomagnetic field. The oscillations of the telluric field originated by tides were first predicted by Faraday in 1832. The physical phenomena that explain those oscillations are connected to the tidal water movement in the earth's geomagnetic field. This phenomenon has been used to estimate average water mass transport in straits, channels, throats or even in the open ocean, using submarine cables. However, the telluric field induced by tides that spreads out far inland could be used to characterize tidal phenomenon. This result opened the possibility to estimate mass transport alongshore associated with tidal flow using onshore measurement of the telluric field.

A review of the fundaments, processing and interpretation of telluric oscillations with tide origin is presented and discussed in this article. The paper presents results obtained from the analysis of data collected in two different systems located in Portugal: 1) a submarine cable crossing the channel at the entrance of a lagoon (Aveiro, Portugal) and, 2) two antennas installed close to the coast line (Portuguese west coast). Spectral analysis of the data revealed that measured voltages are dominated by semidiurnal M_2, S_2/K_2 periods. Values of 720 $m^3\ s^{-1}\ mV^{-1}$ and of 3.0×10^4 and 4.25×10^3 were estimated for the coefficient relating voltage and water transport at Aveiro channel and at the two different sites in the coast line, respectively. The results show that it is possible to indirectly measure the water transport by tidal flow

* E-mail address: fasantos@fc.ul.pt. Instituto Don Luíz-Laboratório Associado, Universidade de Lisboa,Campo Grande, Ed. C8, 1749-016 Lisboa,Portugal

measuring onshore differences of electrical potential. The method shows great potential for low cost accurate long-term monitoring of integral water transport.

Introduction

Sea water flow through the Earth's magnetic field induces secondary electric fields, electric currents and secondary magnetic fields that have a potential for the remote sensing of ocean flow variability, as noted by several authors (see, e.g., Palshin et al. 1996, Tyler et al. 1999, Maus and Kuvshinov 2004). Magnetic field variations, particularly those originated by periodic tidal motion, have been observable in land observatories and satellites, generally with magnitudes of a few nT (see, e.g., Malin 1970, McKnight, 1995, Tyler et al. 1997, 2003). Secondary electric fields generated by tidal movements have been observed in the sea (e.g., Duffus and Fowler 1974, Larsen 1985, Fujii and Utada 2000, Monteiro Santos et al. 2002) and on land and has a potential for electromagnetic soundings of the Earth (Rooney 1938, Harvey et al. 1977, Junge 1988, Monteiro Santos et al 2007).

The oscillations of the electric field originated by tides were first predicted by Faraday in 1832 and observed by Egedal in 1937. The physical phenomena that explain those oscillations are connected to the tidal water movement in the earth's geomagnetic field (Longuet-Higgens 1949, Sanford 1971). This phenomenon has been used to estimate average water mass transport in straits, channels, throats or even in the open ocean, using submarine cables (Harvey et al. 1977, Flosadottir and Taire 1997, Palshin et al. 1999, 2001, Monteiro Santos et al. 2002, 2007, Nolasco et al. 2006). In 1988, Junge demonstrated that the telluric field induced by tides that spreads out far inland can be used to characterize tidal phenomenon. This result opened the possibility to investigate tidal characteristics and to estimate mass transport alongshore associated to tidal flow using onshore measurement of the telluric field.

A review of the theoretical fundamentals, processing and interpretation of telluric oscillations with tide origin measured in narrow channels using short-submarine cables and on land, is presented in this article. The paper presents results obtained from the analysis of data collected in two different systems: 1) in a channel at the entrance of a lagoon (Aveiro, Portugal) and, 2) in two antennas installed close to the coast line (Portuguese west coast). The results show that it is possible to indirectly measure the water transport by tidal flow measuring on shore differences of electrical potential.

Theoretical Fundamentals of the Motionally Induced Voltage (MIV)

Electromagnetic fluctuations in the ocean have external sources and internal, purely oceanic sources, associated with interaction between water velocity fields and the earth's magnetic field. Motionally induced voltage (MIV) phenomenon is generated by movements of free electrical charges through the earth magnetic field. The charged particles in the water having a movement component perpendicular to the vertical component of the earth's magnetic field are deviated by the Lorenz force. The phenomenon was first studied in 1832

by Michael Faraday who also quantified the electrical field $\vec{E}'$, induced by the charge q+ (or q-) moving through the magnetic field $\vec{B}$ with a velocity $\vec{v}$:

$$\vec{E}' = \vec{v} \times \vec{B} \tag{1}$$

Positively and negatively charged particles having a movement component perpendicular to the vertical component of the earth's magnetic field are deviated in opposite direction generating electrical fields that spread far inland. It is thus possible, at least theoretically, by measuring $\vec{E}'$ and $\vec{B}$, to deduce the velocity of water currents, since these in general carry electrical charges in the form of dissolved ions. The characteristics of this field depend on: 1) the water flow and the electric properties of the water and 2) the electric structure of the earth in the area. This phenomenon has been used to estimate average water mass transport in straits, channels, throats or even in the open ocean, using submarine cables (Larsen 1992, Harvey et al. 1977, Flosadottir and Taire 1997, Palshin et al. 2001, Palshin et al. 2002, Monteiro Santos et al. 2002, Fristedt et al. 2002, Nolasco et al. 2006).

The theory of motional induction applicable to the ocean has been developed by many authors, (i.e., Larsen 1968, 1971, Sanford 1971, Filloux 1987, Chave and Luther 1990, Lanzerotti et al. 1992). There are two principal modes for electric currents generated by ocean movements: the toroidal mode, with the currents restricted to the vertical plane and the poloidal mode that includes the currents that are in the horizontal plane. The toroidal mode is the most important one and describes the electric currents in the surface layer forced by surface flow and has weaker returning currents in the deep ocean (Szuts 2008). The poloidal mode exists where gradients in the downstream direction exist. This mode will not be described in this chapter.

Sanford (1971) presented a general theory for MIV assuming: 1) a horizontal ocean bottom (H) with small topography perturbations (h/H << 1), 2) width scales (L) larger than the bottom depth (H/L << 1), 3) predominance of horizontal oceanic movements ($\vec{v} = \vec{v}_h$), 4) distant lateral boundaries, 5) a sedimentary layer with uniform electrical conductivity, and 6) negligible magnetic self-induction and mutual induction. As pointed out by Sanford (1971), the induction parameter $\mu\omega\sigma L^2$ (μ is the magnetic permeability, σ is the electrical conductivity and ω the frequency) must be less than 1 for mutual induction to be negligible. It means that this phenomenon can be discarded for periods longer than 10 hours (Chave and Luther 1990).

The electrical field in a reference frame fixed to the sea floor, is (Sanford, 1971):

$$\vec{E} = \frac{\vec{J}}{\sigma} - \vec{v} \times \vec{B} \tag{2}$$

where $\vec{v} \times \vec{B}$ is the motional field associated with the velocity field $\vec{v}$, $\vec{J}$ is the electric current density and $-\vec{J}/\sigma$ is the resistive or ohmic force opposed by the environment to electric current flow. The form for horizontal electric current divided by conductivity is (Sanford 1971, Szuts 2008),

$$\frac{\vec{J}_h}{\sigma} = (\vec{v} - \bar{v}^*) \times B_z \hat{k} - \nabla_h \left[\frac{1}{H(1+\lambda)} \int_{-H}^{0} \hat{k} \cdot (\vec{v} \times \vec{B}) z' \, dz' + \int_{-H}^{z} \hat{k} \cdot (\vec{v} \times \vec{B}) \, dz' \right] \tag{3}$$

with

$$\bar{v}^* = \frac{\int_{-H+h}^{\varsigma} \sigma \vec{v} \, dz'}{\int_{-H_s}^{\varsigma} \sigma \, dz'} \tag{4}$$

where ς is the sea surface, $\hat{k}$ is the unitary vector in Z direction, $-H$ is the mean depth of the seafloor, h is the perturbation of the seafloor, λ is the sediment conductivity factor and $-H_s$ is the bottom of the conductive sediment. $\bar{v}^*$ is the conductivity-weighted vertically-average velocity and it is linearly related to the vertically averaged velocity. λ is the sediment conductance factor and is given by

$$\lambda = \frac{\int_{-H_s}^{-H+h} \sigma(z) \, dz}{\int_{-H+h}^{\varsigma} \sigma(z) \, dz} \tag{5}$$

From equation (3) the electric current density divided by σ has two terms. The first one is equal to the difference between the current density driven by the vertically uniform electric field and that generated by local horizontal water motion, $(\vec{v}(z) - \bar{v}^*) \times B_z \hat{k}$ (Szuts 2008). Considering baroclinic flows and that the width L of the current is much larger than the depth H, the resulting horizontal electric field is vertically uniform and is given by $\bar{v}^* B_z$. For a non-stratified water $\bar{v}^*$ becomes $\bar{v}^* = \bar{v} / \Sigma$, where $\Sigma = 1 + \lambda_s / \lambda_w$. λ_w and λ_s are, respectively, the conductances of sea-water layer and the ocean bottom sediments and $\bar{v}$ is the mean velocity (Sanford 1971).

The second term of (3) depends on horizontal gradients of topography and of the velocity field. Horizontal gradients of H, λ and $\bar{v}$ can make this term a non-zero term and, frequently, the assumption of small horizontal gradients is invalid. Therefore, high order terms must be took into account in specific areas of the ocean where those condition are verified (Szuts 2008).

Absolute electric fields can be measure using stationary instrumentation such as submarine cables. In this case the local velocity ($\vec{v} \times \vec{B}$) cancels part of the first term of (3) leaving only the electric field caused by v^*, e.g., $\vec{E}_h = \bar{v}^* B_z$. The difference of electric potential between the terminals of a cable (with a distance between end electrodes of L) placed perpendicularly to the water flow depends basically on: i) the telluric field (electric),

generated by the variations of the geomagnetic field; ii) the water flow rate and the electric properties of the fluid and, iii) the electric structure of the terrain in the site (e.g., Sanford 1971, Filloux 1987). In this way, the monitoring of that potential will provide an indirect knowledge of the flow rate and of the mass transport associated with this flux (e.g., Lanzerotti et al. 1992). The induced voltage should be proportional to the average transport ($t = \bar{v}LH$):

$$\frac{t}{\Delta V} = \frac{H\Sigma}{B_z} \tag{6}$$

Therefore, the recording of the variation of the electrical potential between the terminals of the cable will allow us to obtain a measure of the variations of the mass transport with time, and hence, its seasonal and even interannual variations.

Data Processing

The electrical potential difference (*dop*) between a pair of electrodes must be processed before any interpretation. The data are processed with several objectives. For example, moving average of the *dop* data is commonly used to suppress outliers in the time-series. The amplitude spectrum of the averaged electrical potential allows identifying the main spectral components in the recorded signal. The spectrum of the voltages measured in a cable is dominated by semidiurnal M_2, S_2/K_2, P_1/K_1, O_1 and M_4 components (Figure 1). The constituents M_2, N_2, O_1 and M_4 are mainly of oceanic tidal motional origin. The constituents S_2/K_2 and P_1/K_1 are a combination of oceanic tidal motion and geomagnetic origin.

If the main objective is the use of MIV for tidal studies, a calibration coefficient relating the motionally induced voltage of lunar origin (MIVL) and the water transport of the lunar constituents of tides must be estimated. Therefore, the focus will be on the four (M_2, N_2, O_1, M_4) constituents of lunar origin. Let us to consider the signal measured in a cable crossing a narrow channel. Firstly, the different components of the measured signal must be separated. For such the *dop* measured time-series is approximated by a set of lunar harmonic constituents using the least square fitting (LSF) method (Pawlowicz et al. 2002). Sea surface elevation (SSE) measured at a tide gauge can be used to calibrate the cable. In this case, harmonic constituents of lunar origin (M_2, N_2, O_1 and M_4) should be calculated from SSE using the same least square fitting method and the water flow for each component must be estimated. The water flow with lunar origin is then correlated with MIVL measurements allowing the estimation of a calibration factor. The correlation of MIVL can also be done with independent flow measurements or with water flow values obtained from a previously calibrated hydrodynamic model (Nolasco et al. 2006).

Differences of potential measured on shore can be processed and analyzed in a similar way (Marta-Almeida et al. 2010). The separation of the signals in very low frequency and high frequency components can be done by Singular Spectrum Analysis (Marques et al 2006). High frequency component is usually analyzed using Fourier analysis in order to study the components contained in the *dop* signal. Specific analysis of tides components can be done using harmonic fitting (Pawlowicz et al. 2002), as exposed before. Also, the possible

variation of tidal parameters can be investigated making harmonic fit using 60 days moving window (Marta-Almeida et al. 2010).

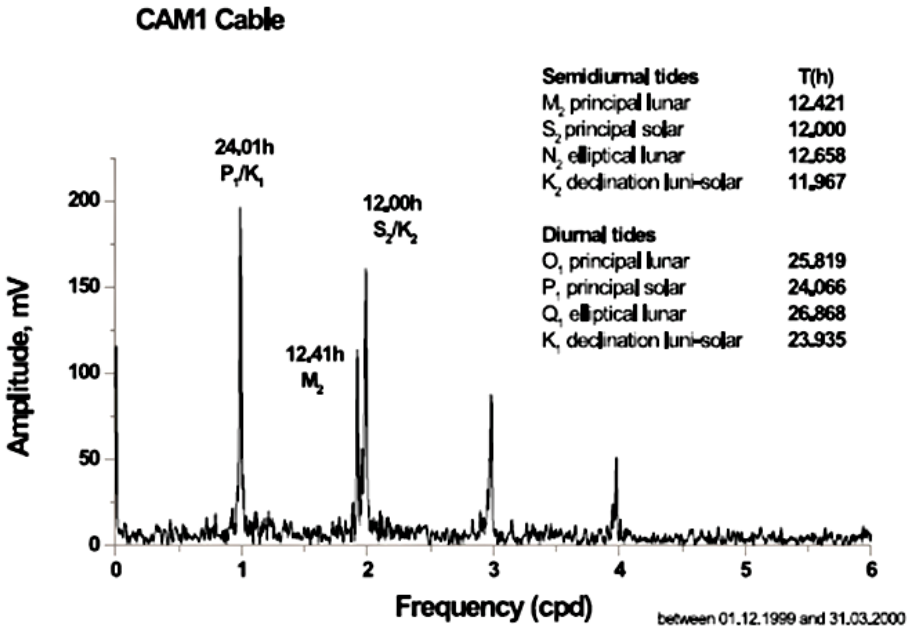

Figure 1. Amplitude spectrum from data collected in the submarine cable CAM-1 between Sesimbra and Madeira Island. From Monteiro Santos et al. (2002).

Case Studies

MIV Measurements in Estuarine Environments Using Submarine Cables

Coastal and estuarine environments are nowadays recognized as significant for bio-diversity evolution. The biotas in these environments are extremely sensitive to changes in water properties. This perception has originated a large research activity in order to understand the parameters controlling the dynamics of those systems. Water flow into the ecosystem is one of the significant physical parameters that need to be monitored and MIV can be used for that.

The Ria de Aveiro (Northwest Portugal) is an example of this kind of system. It is a shallow water lagoon with a very complex geometry, connected with the Atlantic Ocean through a single artificial channel, the Barra channel of 300 m width and from 3 to 25 m depth (Figure 2). All of its water exchange with the ocean takes place by input/output across this narrow entrance. The current velocity varies from 0 to 3 m s^{-1} with typical values of about 1–1.5 m s^{-1} (Dias et al. 2003). The input of fresh water comes from several small rivers distributed by different channels of the lagoon. These characteristics make Ria de Aveiro an ideal place to implement and test innovative sensing systems dedicated to monitoring estuaries and coastal zones (Nolasco et al. 2006).

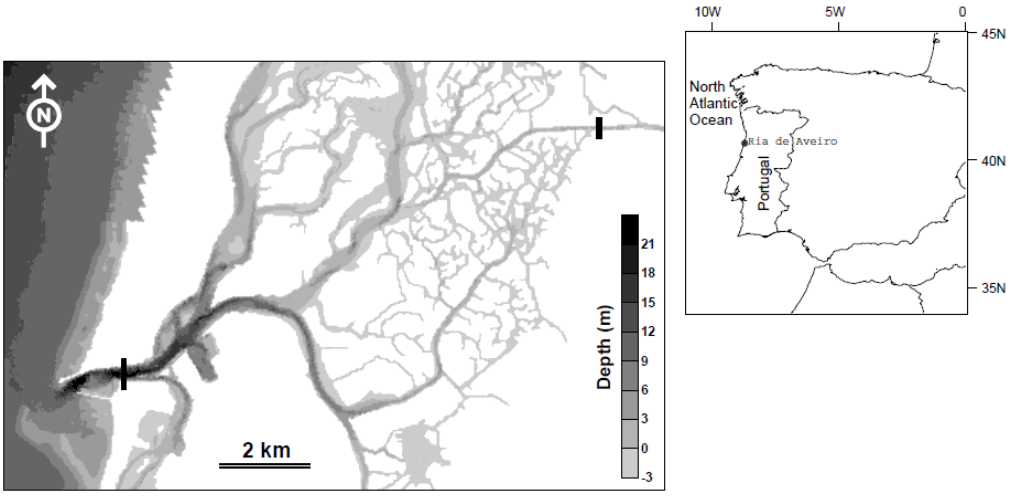

Figure 2. Location of the cable at the Ria de Aveiro. From Nolasco et al. (2006).

A system composed of two silver-silver-chloride (Ag/AgCl) nonpolarizable electrodes, connected to a voltmeter by submarine cables, was installed at the Barra channel (entrance of the lagoon), to allow the estimation of the water transport/flow at this site. The electrodes were specially designed for sea applications and the distance between them was 280 m. The electrical potential difference between the two electrodes was measured using a 16-bit datalogger. The sampling rate of the datalogger was 10 s, but only the average of six values over 60 s was recorded. The main objective was to test the possibility of using the MIV method at Ria de Aveiro to calculate the water transport (by tidal) through Barra channel from the differences of electrical potential measured across the channel.

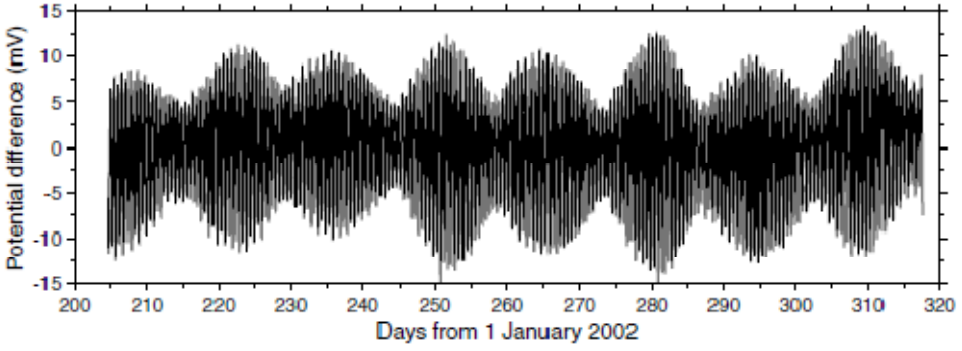

Figure 3. Voltage no cabo em Aveiro (hourly mean values). From Nolasco et al. (2006).

Figure 3 shows the electric potential difference (hourly means) recorded during approximately four months in 2002, across the channel at Barra. The potential difference varies between about −13 and 13 mV. Hourly mean values have been computed to suppress outliers in the time-series. The amplitude spectrum of the hourly mean electrical potential differences is plotted in Figure 4. The spectrum of the measured voltages is dominated by semidiurnal M_2, S_2/K_2 frequencies. P_1/K_1, O_1 and M_4 frequencies are also present, with

smaller amplitudes. The M2 constituent amplitude is higher than the S_2/K_2 or any other frequency in the spectrum. This means that the tidal, M_2, induced electric field is stronger than other constituents of the electric field. The time series also provides the visualization of the spring-neap tidal cycle and the diurnal-inequality characteristic of mixed tidal regime (Figure 3).

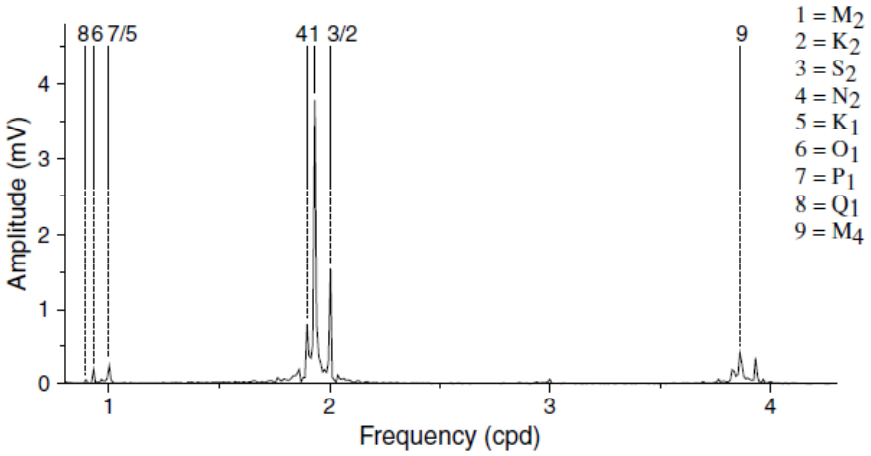

Figure 4. Amplitude spectrum calculated from *dop* recorded at Barra. From Nolasco et al. (2006).

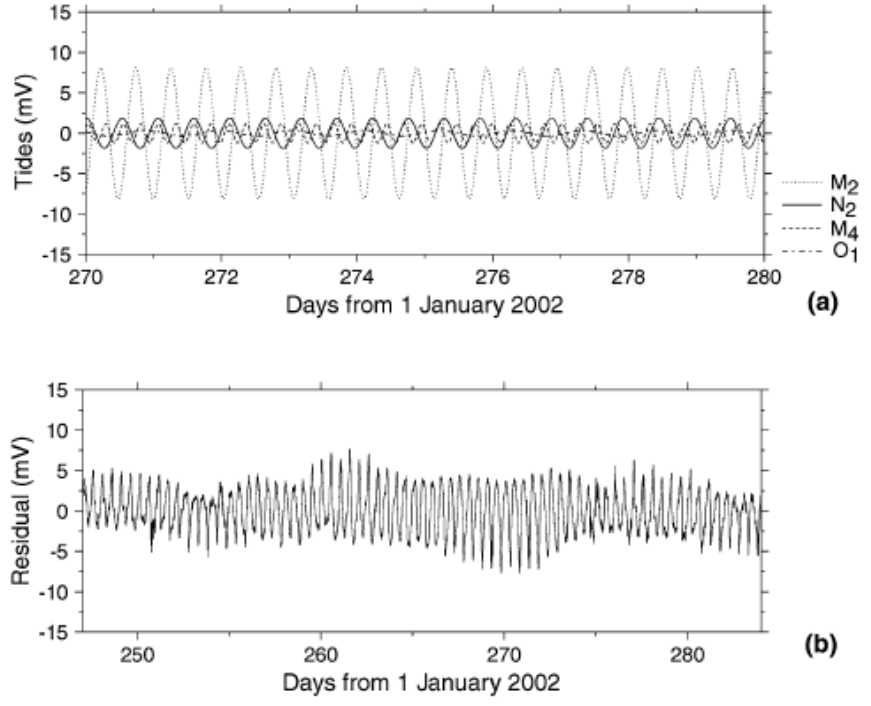

Figure 5. Results of the LSF analysis of the hourly mean dop data collect at Barra. (a) The selected four components with lunar origin (MIVL). (b) Residual time-series obtained after removing the sum of the MIVL components. From Nolasco et al. (2006).

The measured time-series were processed according to the method detailed before: e.g., the series were approximated by a set of lunar harmonic constituents using LSF method (Nolasco et al. 2006). The results of LSF are presented in Figure 5 where Figure 5(a) shows the four lunar constituents with 95 per cent confidence interval and Figure 5(b) presents the residual time-series calculated as the difference between recorded data and MIVL.

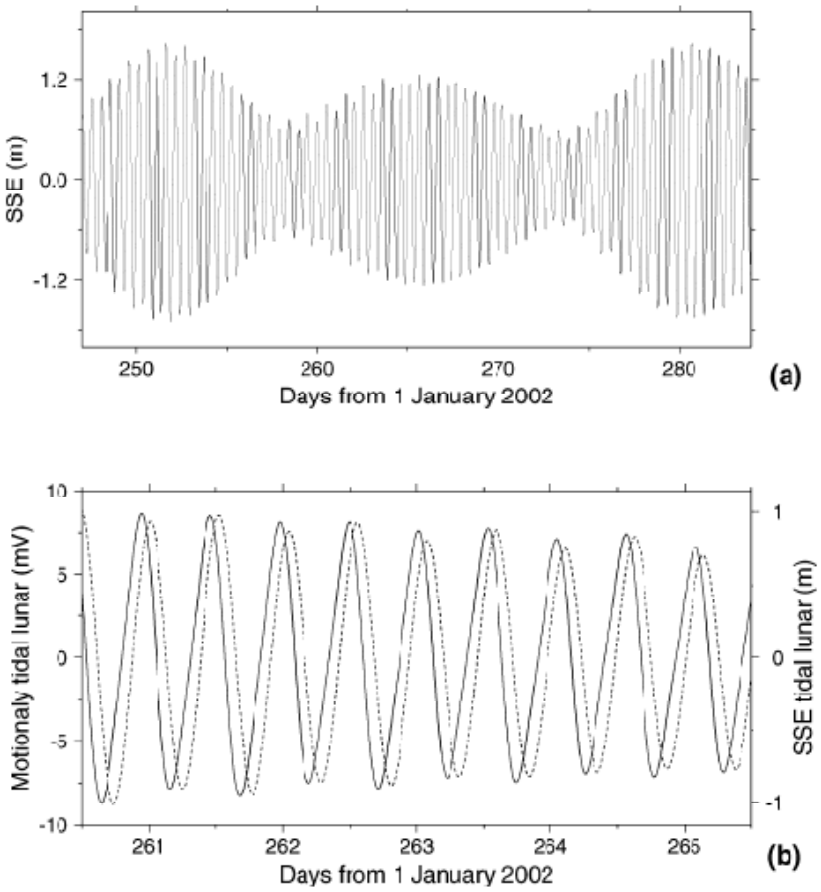

Figure 6. (a) Sea surface elevation (SSE) measured at the tide gauge. (b) MIV*L* in solid line, and the resulting of the sum of the significant harmonics of the SSE in dashed line. The time lag between the two series is about 0.088 days. From Nolasco et al. (2006).

Sea surface elevation from a tide gauge located at the southern side of the channel were digitized, using a sample rate of 1 hr (Figure 6(a) and processed in the same way in order to obtain the harmonic constituents of lunar origin (M_2, N_2, O_1 and M_4). Figure 6(b) shows the sum of the constituents with lunar origin (dashed line). A difference of 0.088 days between the maximum values of electric potential difference and SSE (sums of the lunar constituents) can be noted. Dias (2001) analyzed the delay of the local current inversion relative to high and low water at the lagoon mouth, for both neap and spring tide conditions, based on numerical modeling results. Dias has observed that tidal elevations and velocities are usually not in phase and that high water occurs before high slack tide and low water before low slack tide. The values found are not the same for the high water and the low water cases, ranging

from about 70 min (high water of neap tide) to about 120 min (low water of spring tide). Therefore, the phase shift determined from MIVL and SSE analyses (0.088 days or about 127 min) is consistent with the numerical results. The phase shift is originated by the balance between the pressure force due to the slope of the water surface, and the retarding force resulting from bottom friction (Dias 2001).

As our objective is to correlate water flow/mass transport with the *dop* measured in the cable, we need to have an independent estimation of the water flow/mass transport. In the absence of water fluxes measurements at the mouth of the lagoon in the Barra-Atlantic Ocean channel, results from a 2-D vertically integrated hydrodynamic numerical model (Dias 2001) were used. The program was properly calibrated for Ria de Aveiro lagoon through comparison between model results and measurements of sea surface elevation and current velocity, for several stations distributed along the main lagoon channels (Dias 2001; Dias and Lopes 2006). The model results describes the depth-averaged circulation in a tidal basin, and allows the determination of the sea surface elevation, current velocity and water fluxes in any area of the computational domain.

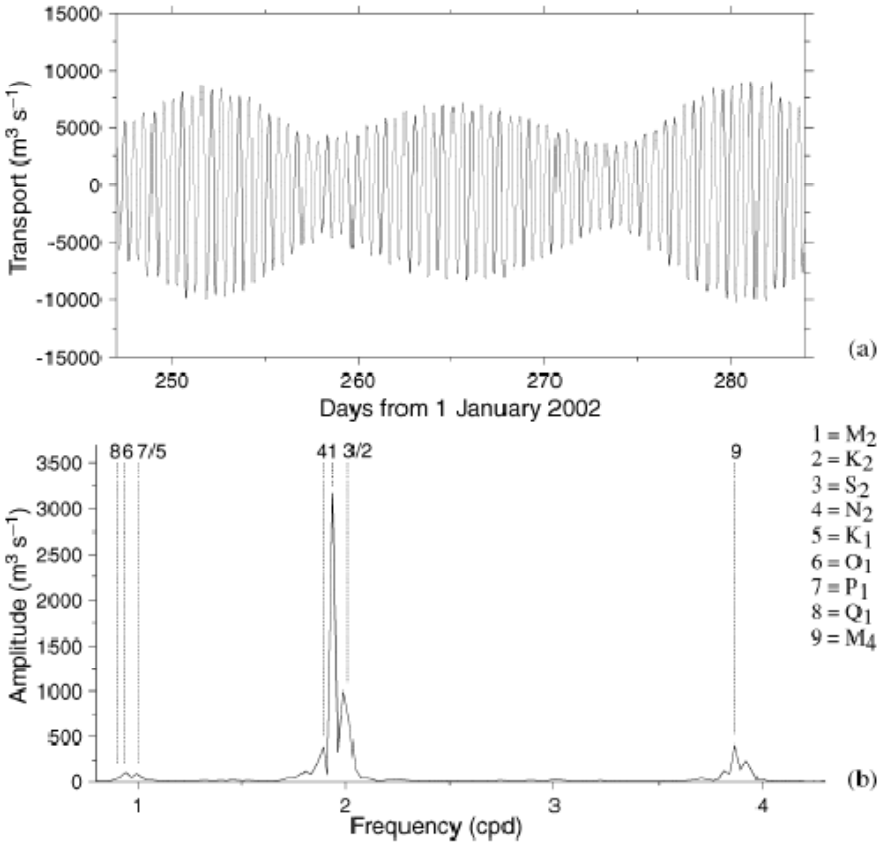

Figure 7. Water transport computed by the hydrodynamic numerical model (a) and its amplitude spectrum (b). From Nolasco et al. (2006).

The water transport time-series computed by the numerical model for the transversal section corresponding to the cable location and the water transport amplitude spectrum are

displayed in Figures 7(a) and (b), respectively. As expected, different tidal constituents, with oceanic moon and sun origin and respective combinations, are identified in the water transport spectrum. In order to obtain the water transport with tidal lunar origin (M_2, N_2, O_1 and M_4), the model time-series was approximated by a set of lunar harmonics using the statistical least square fitting (LSF) method (Pawlowicz et al. 2002). Again the same data processing procedure used regarding the electric potential difference and the SSE data was used. Figures 8 shows the relation between the sum of the four oceanic constituents of the electric potential difference (MIVL) and the sum of the four constituents of the water transport, for the same time period. The best-fit line, in Figure 8, was obtained by least-square method. The correlation between the two time-series allows an estimation of a water transport of 720 m3 s^{-1} for each 1 mV potential difference between the ends of the cable. This coefficient found between both variables allows the calibration of the electrical cable.

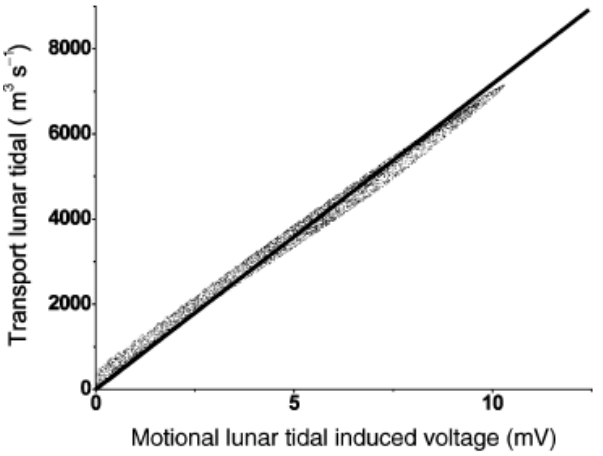

Figure 8. Calibration between motional field due to moon constituents of tides and the correspondent water transport. From Nolasco et al. (2006).

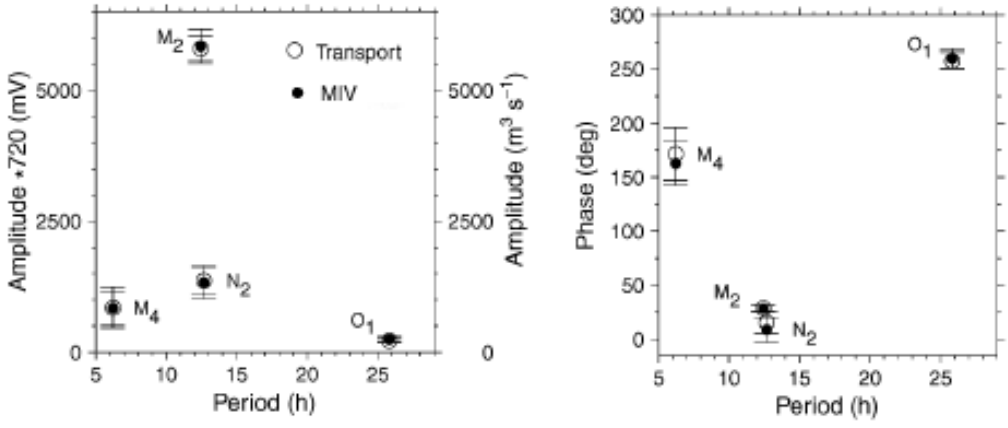

Figure 9. Amplitude and phase of the lunar tidal constituents of the water transport determined by the numerical model and from the MIVL, results of LSF approximation of the data with 95 per cent confidence interval. From Nolasco et al. (2006).

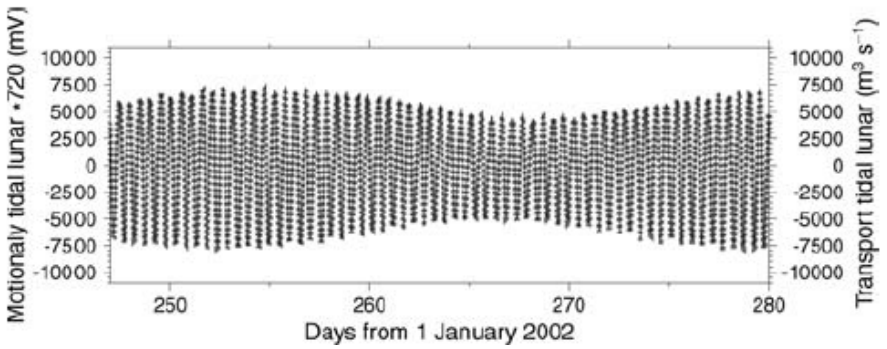

Figure 10. Sums of the lunar tidal constituents of the water transport determined by the numerical model and from the MIVL. From Nolasco et al. (2006).

MIVL values are converted into water transport of lunar origin multiplying them by the calibration factor. Amplitude and phase lag for lunar origin tidal constituents for water transports both numerically computed and determined from the MIVL (with the errors of the LSF for a significance level of 95 per cent), are plotted in Figure 9. The adjustment between both series as regard amplitudes and phases is very good, and small differences between them are included in error bar. As an example of good adjustment of both series, the sums of the lunar constituents for water transports (both numerically computed and determined from the MIVL) are compared in Figure 10.

MIV Measurements on Share around the Ria De Aveiro

An electromagnetic antenna constituted by two pairs of nonpolarizable electrodes (PbPbCl) was installed in the north side of the channel, onshore and close to the Barra. The electrodes were installed in the N–S (approximately N9°E and 360 m apart) and E–W direction (68 m apart) to investigate the possibility to estimate the water transport/ flux in the channel, using onshore electrical potential measurements. They have been placed in salted bentonite in 1.0 to 1.5 m deep holes. The electric potential was sampled at a rate of 10 s, but only the average of six values over 60 s was recorded. Figure 11 shows hourly means of the electric field recorded between days 247 and 317 since January 2002 in the two onshore pair of electrodes. The variations observed in the onshore dipoles are lesser than those observed across the channel in the submarine cable, mainly in the E–W dipole. The electric variations registered on onshore dipoles show a predominantly N–S polarized electric field in the vicinity of the Barra. Since the orientation of the water flow in the Barra channel is predominantly E–W, the N–S electrodes are the most sensible pair of the onshore antennas to the electric signals originated by water transport in the channel.

The amplitude spectrums of the hourly mean electric field are shown in Figure 12. The spectrums are dominated by the same frequencies that are present in the submarine cable. However, the small importance of the M_2, S_2/K_2 frequencies should be noted. The 3 cpd (8 h) tidal component is present in the onshore measured fields but is not revealed in the cable data. Moreover, the 4 cpc (6 h) tidal component, corresponding to shallow water harmonics, is shown in the N–S cable spectrum and is absent in the E–W and cable measured fields. The spectrum for the E–W dipole shows that this component is noisier than the N–S one.

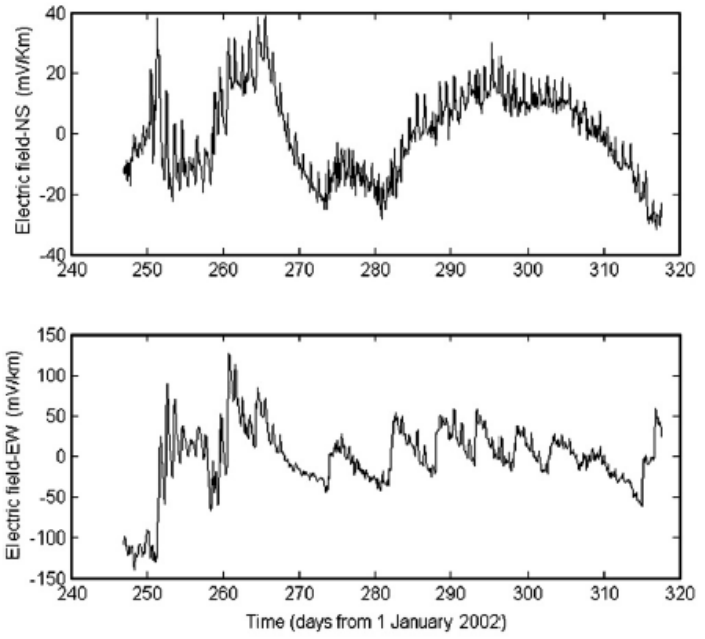

Figure 11. Hourly mean of the electric field measured in the N–S onshore dipole (top) and with the E–W onshore dipole (bottom). From Monteiro Santos et al. (2007).

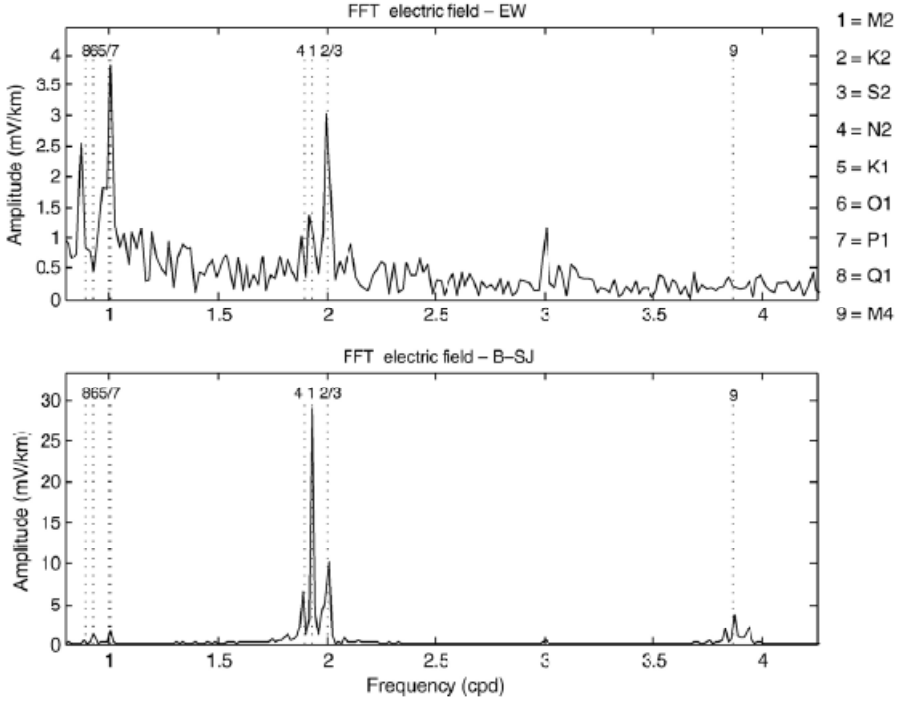

Figure 12 . Amplitude spectrum obtained from data recorded with the N–S dipole (top) and the E–W dipole (bottom). From Monteiro Santos et al. (2007).

The main objective is to use onshore electric potential measurements in the vicinity of a channel to evaluate the mass transport for the water flow in the channel. Therefore, let us concentrate our attention into the M2 component in the antenna. In order to separate this component from the total signal, the measured time series were approximated by a set of lunar harmonics constituents using the least square fitting method, as explained before. A detailed explanation of the method is presented in Nolasco et al. (2006). The results obtained are presented in Figure 13 where amplitude and phase lag for tidal components for water transport, electric field in the submarine cable and in the onshore dipoles (with the errors of the least square fitting) are plotted. The adjustment between the series regarding amplitude and phases is very good, except for the E–W onshore dipole where a significant error is observed.

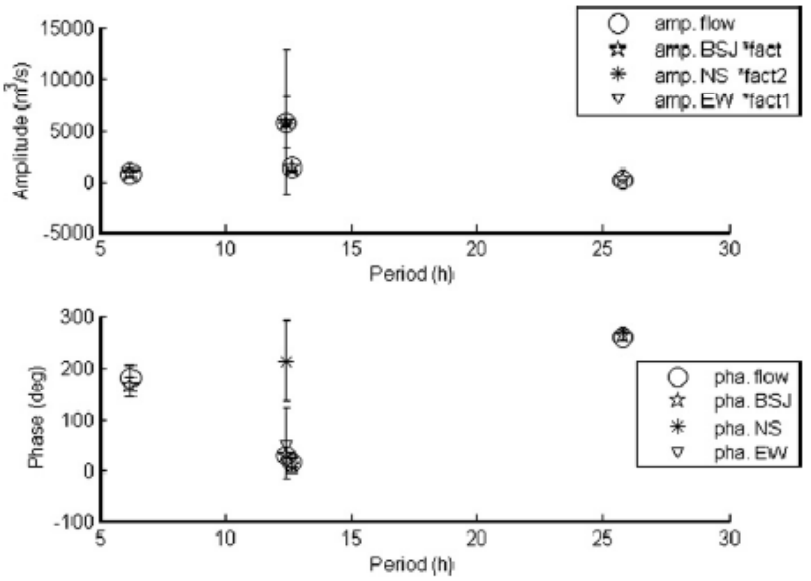

Figure 13. Amplitude and phase of the lunar tidal constituents for water transport, electric field in the submarine cable and on-shore dipoles determined by least square fitting approximation of the data with 95% confidence interval. From Monteiro Santos et al. (2007).

As the *dop* measurements in the onshore antennas and in the submarine cable were carried out simultaneously the results from both systems can be analyzed together in order to estimate the calibration coefficient for the onshore antennas (Monteiro Santos et al. 2007). Figure 14 shows the M_2 harmonics of the electric field measured in the submarine cable and in the N–S dipole together with the water flux/submarine cable calibration. A delay of 3.62 h between the maximum values of the water flux and the electric field measured in the N–S dipole can be noted.

Comparing the M_2 component of the electric field measured in the submarine cable with that measured in the N–S dipole, one notes the relation $E_{cable} = 36.46\ E_{N-S}$ between their amplitudes. A calibration factor for the onshore antenna can be estimated using the correlation between the water transport in the channel (or their equivalent electric potential in the cable) and the electric potential differences with tidal origin measured in the N–S dipole.

A value of 7350m^3 s^{-1} for each mV/km in the N–S onshore dipole and of 5476.9m^3 s^{-1} for each mV/km in the E–W dipole was estimated for water transport.

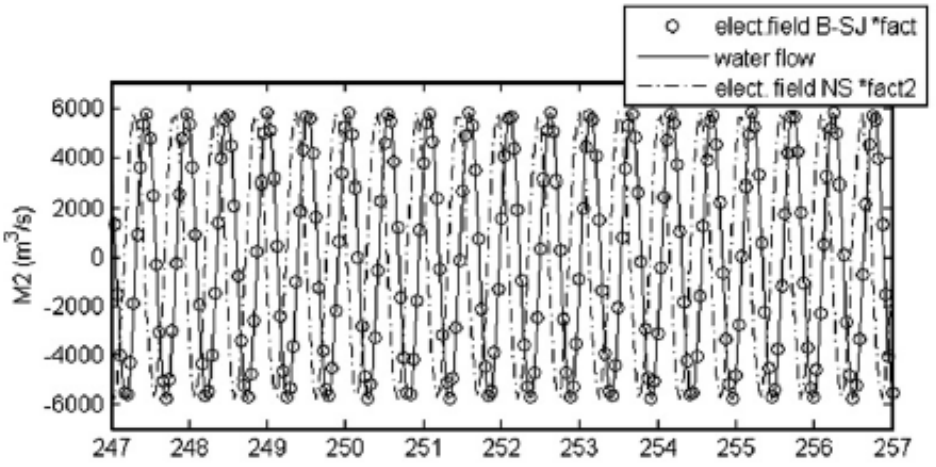

Figure 14. Comparison between the M2 components of the electric field measured with the submarine cable and the N–S dipole with the water transport. The cable electric field values were multiplied by the factor 201.6 m^3 s^{-1} mV^{-1} km, whereas the N–S field values were multiplied by the factor 7350 m^3 s^{-1} mV^{-1} km. From Monteiro Santos et al. (2007).

Modelling

We adopt the model proposed by Junge (2001) in order to explain some of our onshore observations around Ria de Aveiro. Figure 15 gives a schema of the current at the Barra channel with tidal origin for a fixed time t_0. As the ions in the water moves perpendicularly to the vertical component of the earth magnetic field ($\vec{B}$), the charges separation takes place. These charges will cause electric currents in vertical planes in and beneath the water. The scale length of the horizontal water current, characterised by its wavelength λ_y, exceeds the thickness of the uppermost conducting earth layer with an integrated conductivity τ_L. The vertically integrated electric current density $\vec{I}$ is:

$$\vec{I}(x,y,t) = \int_{z_1}^{z_2} \vec{J}(x,y,z,t)dz \tag{7}$$

where z_1 and z_2 are the lower and upper boundary of the conducting layer and $\vec{J}$ is the current density which is given by (Sanford 1971), $\vec{J} = \sigma(\vec{E} + \vec{v} \times \vec{B})$. Integrating (7) we obtain

$$I_L - (\tau_w + \tau_L^{'})E_x = -\tau_w B_z v_y \tag{8}$$

where τ_w and $\tau_L^{'}$ are the integrated conductivities of seawater and conducting sedimentary layer beneath the channel. The right side of the equation (8) is the current source and the left hand side represents the different parts of the resulting currents in the vertical and horizontal planes.

Considering that the current along the "Ria de Aveiro" I_L varies harmonically with the period T_{M2} (= 12.4206 h) and the Greenwich phase φ_{M2} (≈ 28º), the potential $V(P,t)$ at $P(x,y)$ distant of r_P from the current source at y_0, is (Junge 2001)

$$V(x,y,t) = \int_{y_A}^{y_B} V^*(x,y,t;y_0)dy_0 \tag{9}$$

where $V^*(x,y,t;y_0) = \frac{I_L(t)}{\pi\tau_L}\ln(\frac{1}{r_P})$ represents the logarithm potential at P originated by the current I_L at y_0. Here, $r_P = \left[x^2 + (y-y_0)^2\right]^{1/2}$ and

$$I_L(t,y_0) = I_{L0}\sin\left[2\pi(\frac{y_0}{\lambda_y} - \frac{t}{T_{M2}}) + \varphi_{M2}\right] \tag{10}$$

where

$$I_{L0} = h_w\, v\, \sigma_w\, B_z) \tag{11}$$

is the mean maximum amplitude of the integrated electric current density. Therefore, the components of the electric field with motionally origin is (Junge 2001):

$$E_x(x,y,t) = \frac{I_{L0}}{2\pi\tau_L} x\int_{y_A}^{y_B}\frac{1}{x^2+(y-y_0)^2}\sin\left[2\pi(\frac{y_0}{\lambda_y} - \frac{t}{T_{M2}}) + \varphi_{M2}\right]dy_0 \tag{12i}$$

$$E_y(x,y,t) = \frac{I_{L0}}{2\pi\tau_L}\int_{y_A}^{y_B}\frac{y-y_0}{x^2+(y-y_0)^2}\sin\left[2\pi(\frac{y_0}{\lambda_y} - \frac{t}{T_{M2}}) + \varphi_{M2}\right]dy_0 \tag{12ii}$$

y_A and y_B are the limits of integration in the direction of the channel flow. It should be noted that this model does not consider the contribution of the currents parallel to the coast line. In this study and for the Aveiro particular case, it was assumed that these contributions are negligible.

The mean water depth in Barra is 16 m, and its wavelength is about 40 km. The vertical water flow will be assumed as negligible compared to the horizontal one, which will be v_y =1 m/s. The conductivity of the sea water will be considered uniform (3.33 S/m), as well as the water depth and water velocity. The vertical component of the mean magnetic field at the

time of the observations was 36200 nT. Then, the mean maximum amplitude of the integrated electric current density is I_{L0} = 1.9 x 10^{-3} A/m. The water conductance is τ_w = 53.3 S.

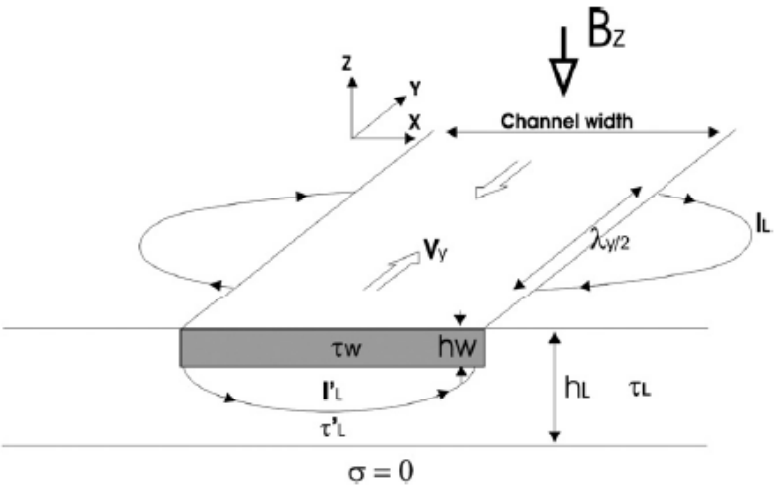

Figure 15. Schematic view of the tidal current in a channel and induced telluric currents at a fixed time (adapted from Junge 2001).

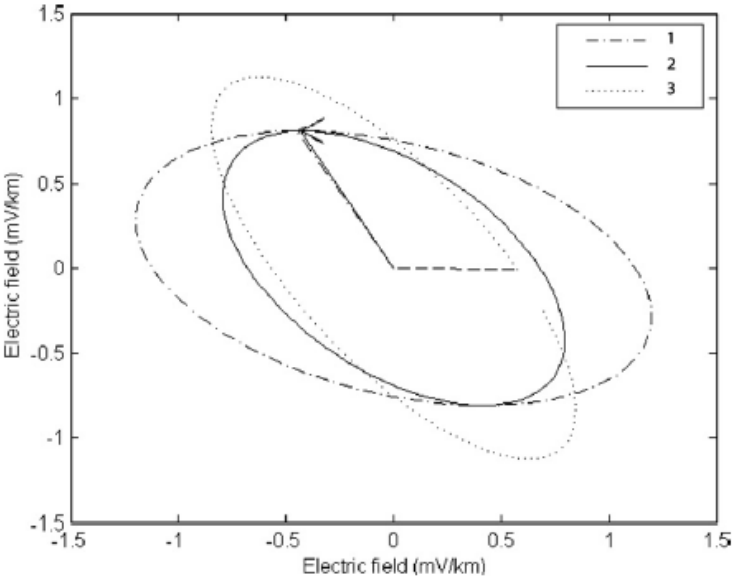

Figure 16. Comparison between observed (solid and dash-point lines) and theoretical (pointed) telluric polarization ellipses. Lines 1 and 2 represent the ellipses calculated using the extreme values of the lunar tides constituents of the E-W electric field component. From Monteiro Santos et al. (2007).

It was observed that the electric field measured in the N-S dipole is about 1/36.46 lesser than the electric field measured in the submarine cable. Our model does not allows for the modelling of the electric field in the cable, therefore we compare the theoretical electric field calculated at the N-S dipole site with that one calculated at a point 5 m apart from the source

current located at northern edge of the channel. The value of τ_L is unknown. For this reason, we proceeded by trial-and-error. A value of 1/32.1 for the ratio $E_{N\text{-}S}/E_A$ was obtained with τ_L = 1200 S. In this case the calculated ratio is closer to the observed value and the conductance value was assumed for the next step.

Figure 16 shows the comparison between the measured and theoretical telluric ellipse calculated at a location corresponding to the middle of the N-S dipole. The figure shows two measured ellipses calculated from the extreme values of the lunar tides constituents of the E-W electric field component. The theoretical ellipse has the major axes approximately in the NNW-SSE direction. The agreement of the theoretical and experimental ellipses can be considered good, taking into account our simplified model and the errors in the E-W electric field component.

MIV Measurements in the West Portuguese Coast (Onshore)

MIV measurements carried out onshore close to the coast line can also be used for tides characterization and alongshore transport estimation. The principle is exactly the same as exposed before: MIV values recorded onshore using two electric dipoles are correlated with estimated/measured tidal transport and a calibration coefficient is calculated. In our experiment the pairs of electrical dipoles were installed close to the sea at two locations along the western coast of Portugal in N-S and E-W directions. The sites, São Jacinto and Sines are indicated in Figure 17. At Sines the electrodes are installed 200 m apart roughly in the direction perpendicular and parallel to the coastline. At São Jacinto the distance between electrodes are 360 m and 68 m for the N-S (9ºE) and E-W dipoles, respectively.

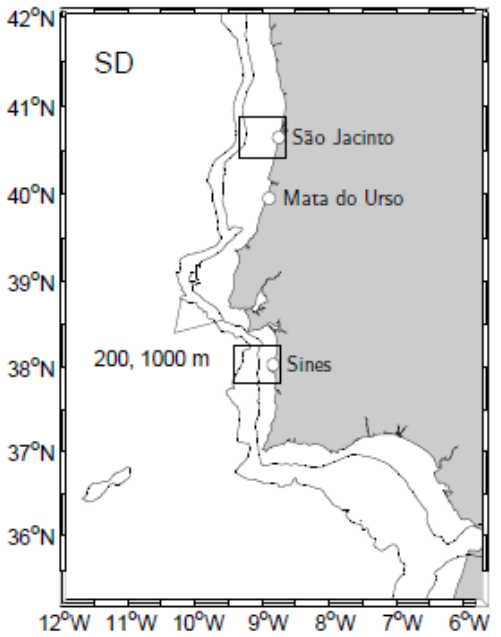

Figure 17. Location of the antennas installed in the West Portuguese coast.

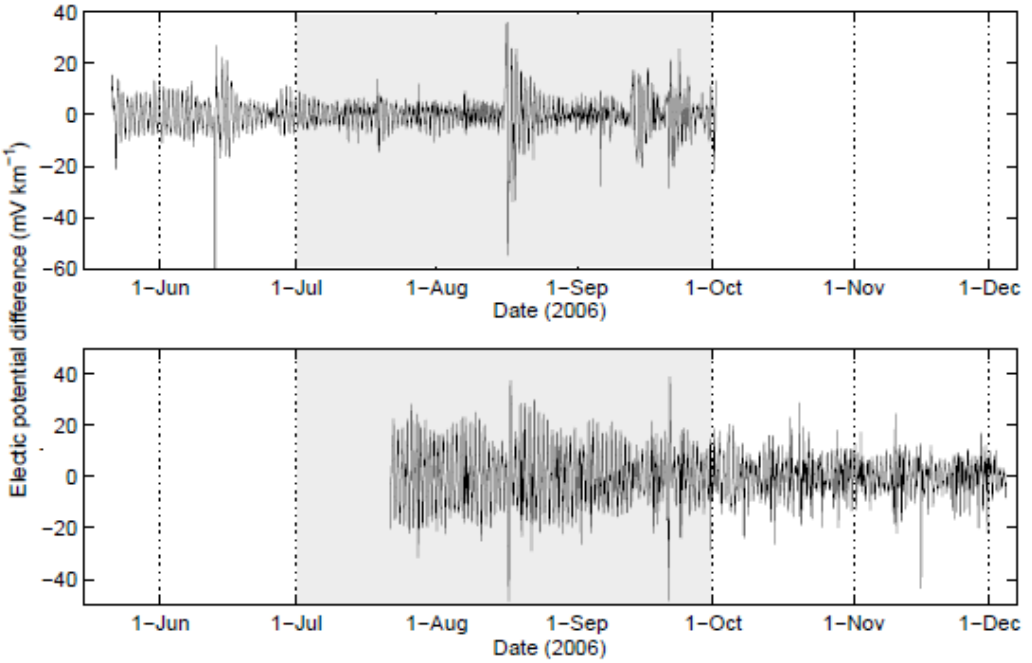

Figure 18. Data from São Jacinto (top) and Sines (bottom) E-W antennas. The shaded regions (1-Jul to 1-Oct) represents the ocean simulations period.

Since the coastline is mainly N-S oriented the electric signal is predominantly sampled by E-W dipoles and the signal observed in N-S dipoles was not used in the present investigation. All the electrodes have been placed in salted bentonite into 1.0 to 1.5 m deep holes. The electric potential difference between electrodes was sampled at a rate of 10 s, but only the average of six values over 60 s was recorded. The distance from dipoles sites and the coastline was about 500 m. The measurements used in this study took place during the Summer and Autumn of 2006.

Figure 18 shows the difference of potential measured in the E-W dipoles located in São Jacinto and Sines after the background long period on the signals has been removed using a Singular Spectrum Analysis algorithm (Marques et al. 2006). The signals have typical amplitudes between 10 and 20 mV km^{-1} for São Jacinto and arround 20 mV km^{-1} for Sines. The signals were explored with Fourier analysis (Figure 19). Both signals have very strong components around the diurnal (stronger) and semidiurnal periodicities. Since the main tidal components in the western Portuguese region are M2 and S2 (Marta-Almeida and Dubert 2006), i.e., semidiurnal, it can be realised that much of the *dop* must have geomagnetic and not oceanic origin. Aiming to quantify the importance of tides in the *dop* signal, the signals were examined with harmonic fit using the tidal analysis package T TIDE (Pawlowicz et al. 2002). The amplitudes and phases (and its estimated errors) of the main lunar components (M2, N2, O1 and Q1) are shown in Table 1.

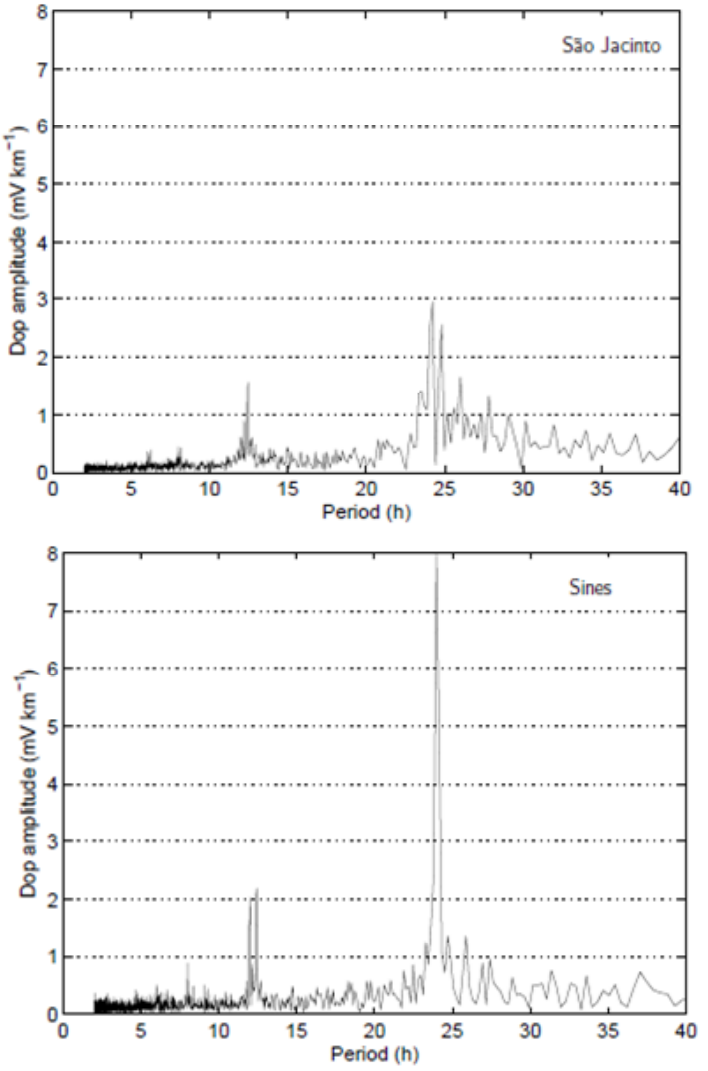

Figure 19. Amplitude spectrum of the dop signals measured in the E-W dipoles installed in São Jacinto and Sines.

Table 1. Tidal analysis of the *dop* signals. Amplitude (amp), amplitude error (eamp), phase (pha) and phase error (epha) of the main lunar constituents for the region, M_2, N_2, O_1 and Q_1. The units are mV km^{-1} for amplitudes and degree for phases.

	São Jacinto				Sines			
	amp	**eamp**	**pha**	**epha**	**amp**	**eamp**	**pha**	**epha**
M_2	2.06	0.52	148.48	15.46	3.39	0.94	61.18	15.68
N_2	0.66	0.56	133.91	50.79	0.73	0.77	17.10	69.96
O_1	0.55	0.99	120.05	121.31	1.22	1.39	344.39	57.23
Q_1	0.72	0.94	59.74	110.72	0.88	1.16	251.85	85.54

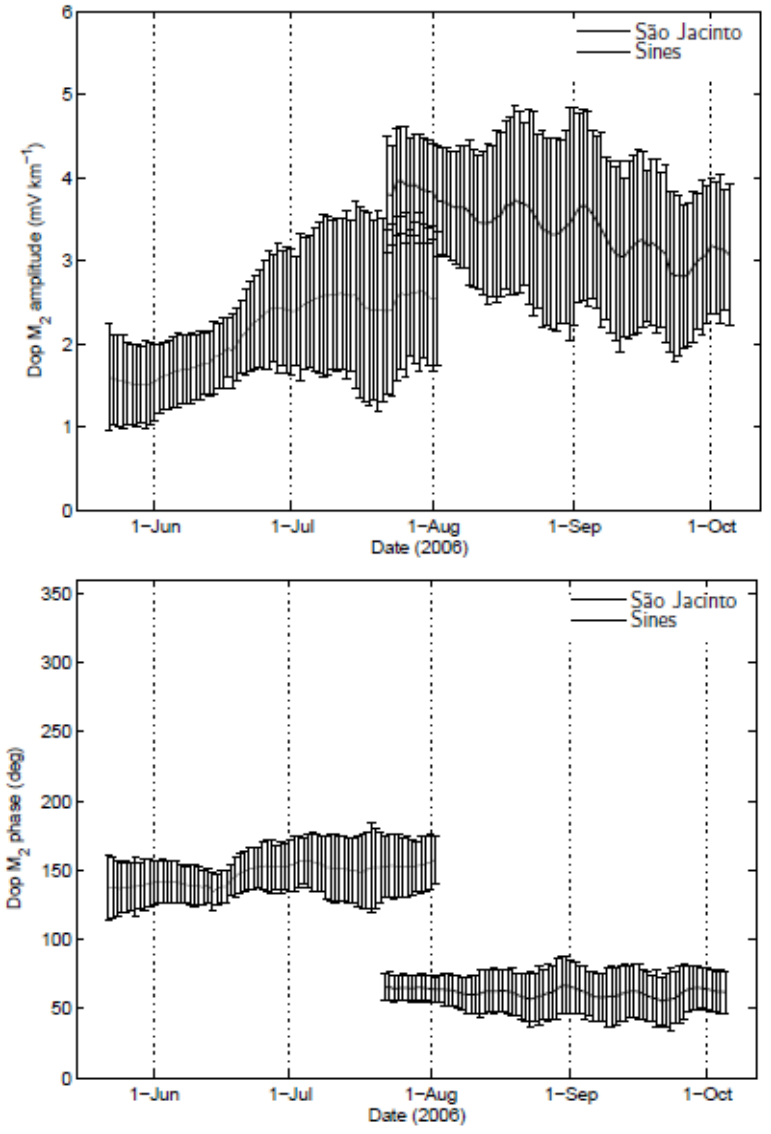

Figure 20. Tidal analysis of the São Jacinto and Sines *dop* signal using a moving 60 days period. The amplitudes (a) and phases (b) refer to the frequencies of the tidal component M_2.

The tidal harmonic fit was repeated using a 60 days moving window, instead of the entire dataset available, with daily increments and starting from the beginning of the *dop* data available for each of the two dipoles (Figure 20) in order to investigate the possible variation of tidal parameters with time. For São Jacinto the M2 amplitude ranges from 1.5 and 2.5 mV km^{-1} with errors around 0.75 mV km^{-1}. Phase ranges between 140º and 160º with errors of about 20º. Amplitude for Sines lays between 3 and 4 mV km^{-1} with errors around 1 mV km^{-1} and the phase is between 55º and 65º with errors of about 15º◦.

In order to establish the relationship between the *dop* measured with electrical dipoles and the oceanic current field, numerical modelling techniques that allows to forecast the tidal and subtidal currents in the coastal zone offshore the dipoles were used. The ocean model

used was the Regional Ocean Modeling System (Shchepetkin and McWilliams 2003, 2005) with embedded nesting capabilities, ROMS-AGRIF (Adaptative Grid Refinement in Fortran, Penven et al. (2006)), a 3D free-surface s-coordinate terrain following primitive equation model with hydrostatic approximation configurable for fully realistic regional applications. ROMS-AGRIF enables the use of online and offline nesting thus permitting regional applications to be built based on large-scale configurations covering a wide range of time and space scales. Previous works of ROMS-AGRIF applications to Western Iberia are reported in Peliz et al. (2007, 2009); Teles-Machado et al. (2007); Marta-Almeida et al. (2008).

With the objective to resolve the shelf circulation of the west coast of the Iberian Peninsula, a nested grids configuration has been implemented for the Summer 2006 (July 1st to October 1st). The nested model was forced with climatological surface fluxes, the surface momentum and heat fluxes data were obtained from simulations with the widely used atmospheric model Weather Research and Forecast, WRF (Skamarock et al. 2005). Surface winds, humidity, pressure, air temperature and radiative data were generated by WRF model and passed to the oceanic model to calculate the air-sea fluxes. Tidal circulation was achieved by imposing a tidal forcing at the boundaries. This forcing consisted in the superposition at the lateral boundaries of tidal parameters for elevations (amplitude and the Greenwich phase) and currents (barotropic tidal ellipses in the form of semi-major and semi-minor axis, inclination and Greenwich phase) from the TPXO database for the North Atlantic (Erofeeva and Egbert 2002). This database provides information for the main diurnal and semidiurnal constituents, M_2 S_2, N_2, K_2, K_1, O_1, P_1 and Q_1, with a resolution of 1/6º. The details and modeling techniques of the tidal dynamics for the region, using a similar approach to the present one, has already been done for the homogeneous case (Marta-Almeida and Dubert 2006).

With the objective of analyse the alongshore (N-S) transports, perpendicular to the installed E-W dipoles, the 3D currents were outputted hourly from the model at every grid points of the higher resolution domain, in an offshore line, from the shore, near the locations of the two dipoles, until the shelf break assumed as the 200 m isobath. The shelf break distance from coast in São Jacinto (Dsj) is about twice the one at Sines (Dsi). For this reason and aiming to analyse transports crossing equal areas we caculated the transport for Sines until the 200 m isobath (Hsi) and for São Jacinto until the isobath for which the cross-shelf areas for both regions are equal (the isobath 114 m, Hsj). This choice of the area was arbitrary without any base than the idea that *dop* signals are more influenced by transports near the dipoles. The transports were calculated for the whole simulation period and the resultant time series were considered as the ocean signals (TR hereinafter), ie, the signals that induced the electric *dop* in the onshore dipoles. For this reason these transports are used to calibrate the dipoles.

Thus, as well as for *dop* signals we decompose the TR signals into high frequency and subinercial components. This step was done with the widely used tidal low-pass filter pl33 (Flagg et al. 1976). For São Jacinto the tidal oscillations have a half-amplitude arround 10 $\times 10^4$ m^3 s^{-1}. For Sines, the amplitudes of the tidal component are about half the amplitudes in São Jacinto (Figure 21).

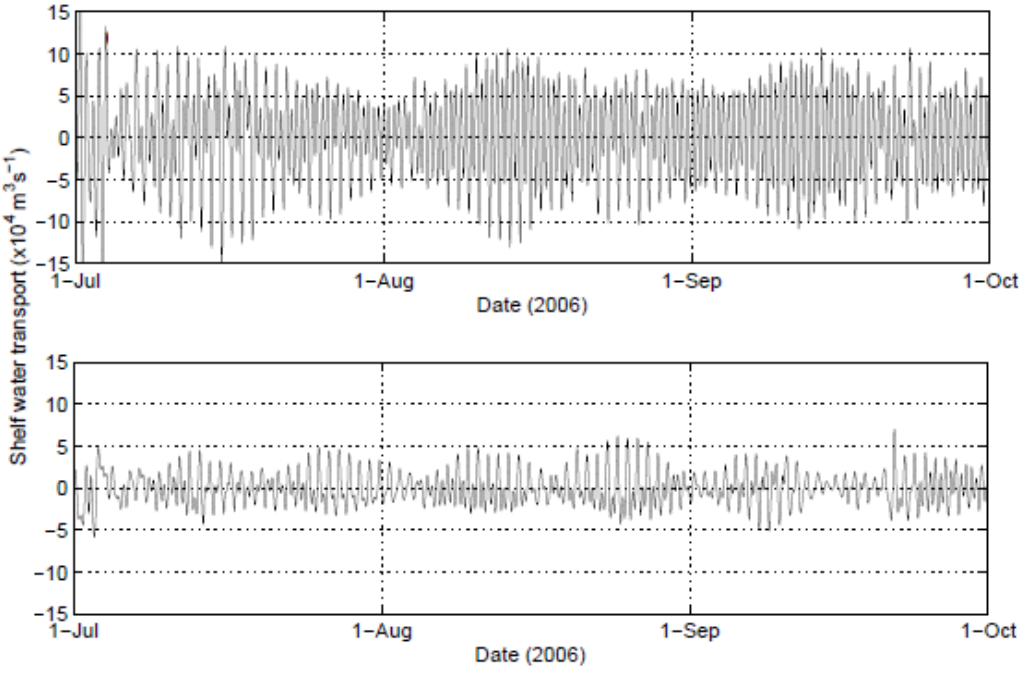

Figure 21. Alongshore shelf water tidal transport component from coast to 200 m isobath adjacent to the dipole of São Jacinto (top) and Sines (bottom).

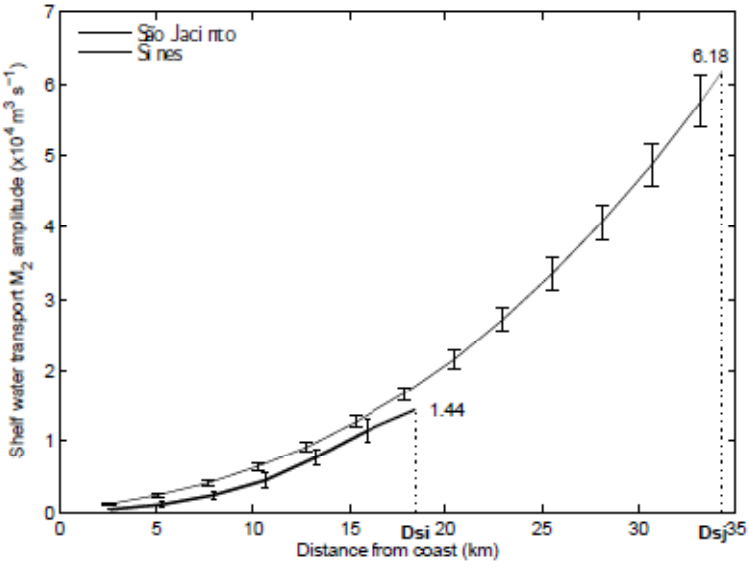

Figure 22. M_2 amplitude of the alongshore shelf sea transport adjacent to the São Jacinto and Sines antennas. The vertical dotted lines indicate the 200 m isobath and the numerical labels at its top are the amplitudes for the distance from coast of the isobath 200 m.

The differences between the two locations, in spite of using the same cross-shelf area, can be explained by the fact that the alongshore current resulting from the adjustment of the M_2

tidal constituent is smaller in the Sines region (Marta-Almeida and Dubert 2006). A tidal decomposition, similar to the described above for *dop* in both sites, was applied to the series of high frequency TR. The amplitudes obtained and its corresponding errors for our tidal constituent of interest, M_2, were 6.18 ± 0.33 $\times 10^4$ m^3 s^{-1} for São Jacinto and 1.44 ± 0.18$\times 10^4$ m^3 s^{-1} for the Sines transport. The corresponding M_2 Greenwich phases found were 265 ± 3º and 129 ± 6º respectively.

Considering the full series of *dop* signal available and the TR transports we obtain a calibration factor for the main tidal frequency, M_2, of $6.16\times10^4/2.06=3.00\times10^4$ m^3 s^{-1}/mV km^{-1} for São Jacinto and $1.44\times10^4/3.39=4.25\times10^3$ m^3 s^{-1}/mV km^{-1} for Sines (Figure 22).

A Simple Model for MVI Measured on Shore

To predict the on shore electric fields due to the tidal ocean flow, we adopt again, the simple model described by Junge (1988, 2001). The solution allows simulating the electric field, measured on shore due to tidal transport parallel to the coastline. This is a simplification of the ocean-land interaction conditions verified in west Portuguese coast and has the objective to estimate the magnitude of the expected magnitudes of N-S and E-W electric field components originated by M_2 tidal movements.

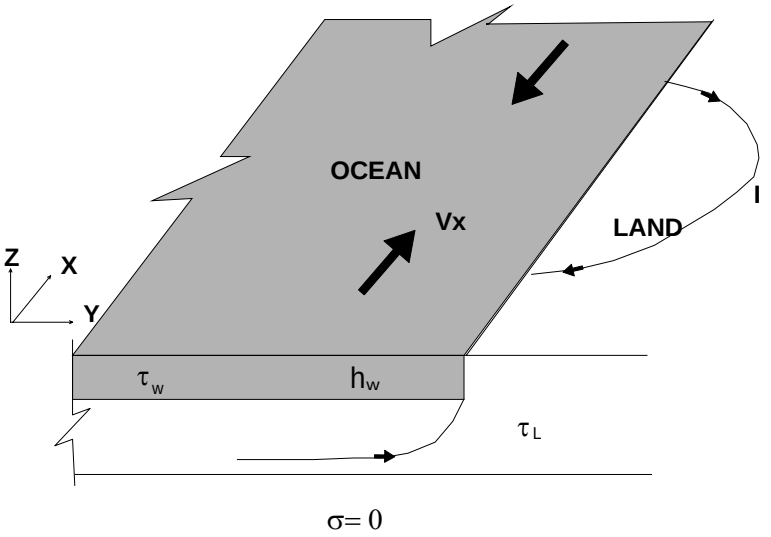

Figure 23. Schematic view of the tidal current in a channel and induced telluric currents at a fixed time (adapted from Junge 2001).

Figure 23 gives a schematic view of the current at the west coast with tidal origin for a fixed time t_0. The scale length of the horizontal water current, characterised by its wavelength λ_x, exceeds the thickness of the uppermost conducting earth layer with an integrated conductivity τ_L. Considering that the current I along the coast varies harmonically with the period T_{M2} (12.4206 h) and the Greenwich phase φ_{M2} (≈20º)

$$I = I_o \sin\left[2\pi\left(\frac{x_o}{\lambda_x} - \frac{t}{T_{M_2}}\right) + \varphi_{M_2} \right] \tag{13}$$

where I_o is the mean maximum amplitude of the integrated electric current density and is given by equation (11), the components of the electric field $\vec{E}(P,t)$ at $P(x,y)$ distant of r_P from the current source at x_0 with tidal origin, are given by equation (12) (Junge 2001, Monteiro Santos et al. 2007). In the adopted referential the components of the electric field are

$$E_x(x,y,t) = \frac{I_o}{2\pi\,\tau_L} \int_{x_A}^{x_B} \frac{x - x_o}{y^2 + (x - x_o)^2} \sin\left[2\pi\left(\frac{x_o}{\lambda_x} - \frac{t}{T_{M_2}}\right) + \varphi_{M_2} \right] dx_o$$

$$E_y(,y,t) = \frac{I_o}{2\pi\,\tau_L}\, y \int_{x_A}^{x_B} \frac{1}{y^2 + (x - x_o)^2} \sin\left[2\pi\left(\frac{x_o}{\lambda_x} - \frac{t}{T_{M_2}}\right) + \varphi_{M_2} \right] dx_o \tag{14}$$

x_A and x_B are the limits of integration in the water moving direction.

Considering that the wavelength is about 12000 km, v_x=1 m/s, seawater conductivity of 3.33 S/m and B_z = 36200 nT, the mean maximum amplitude of the integrated electric current density is $I_o = 1.2\text{x}10^{-2}$ A/m and the water conductance is τ_w = 33.33 S (for a 100 m thick ocean). It must be noted that the earth conductance value (τ_L) is unknown. For this reason we calculated the electric field on shore for different values of τ_L and compared with measured values (Figure 24). Table 2 shows the relationship ($\max E_y / \max E_x$) between the maximum values of the field components measured and calculated in Sines and São Jacinto. There is a very good agreement between observed and calculated values in Sines. At São Jacinto the observed ratio is close to unit, whereas the calculated is 5.72. The reason of this disagreement is the strong influence of the MIV originated by the strong E-W water flow in Ria de Aveiro, which is not considered in this model.

Table 2. Ratio (max E_y)/(maxE_x) in both onshore sites.

	Sines	**S. Jacinto**
Observed	4.35	1.14
Calculated($\tau_{L=8000\ S}$)	4.92	5.72

At Sines both measured components are compatible with τ_L ranging from 5000 to 6000 S. At São Jacinto only the E-W component is compatible with a value around 8000 S for the earth conductance. The N-S component only can be modelled if a conductance of about 2000 S is chosen. This discrepancy is motivated by the fact that the N-S on shore electric component is strongly affected by the water movement in Ria de Aveiro located very close the on shore dipoles, as demonstrated by Monteiro Santos et al. (2007). As explained above the N-S component in São Jacinto is mainly determined by the water flow in the Ria de

Aveiro. The earth conductance value of 1200 S for presented before is compatible with the result achieved in this paragraph.

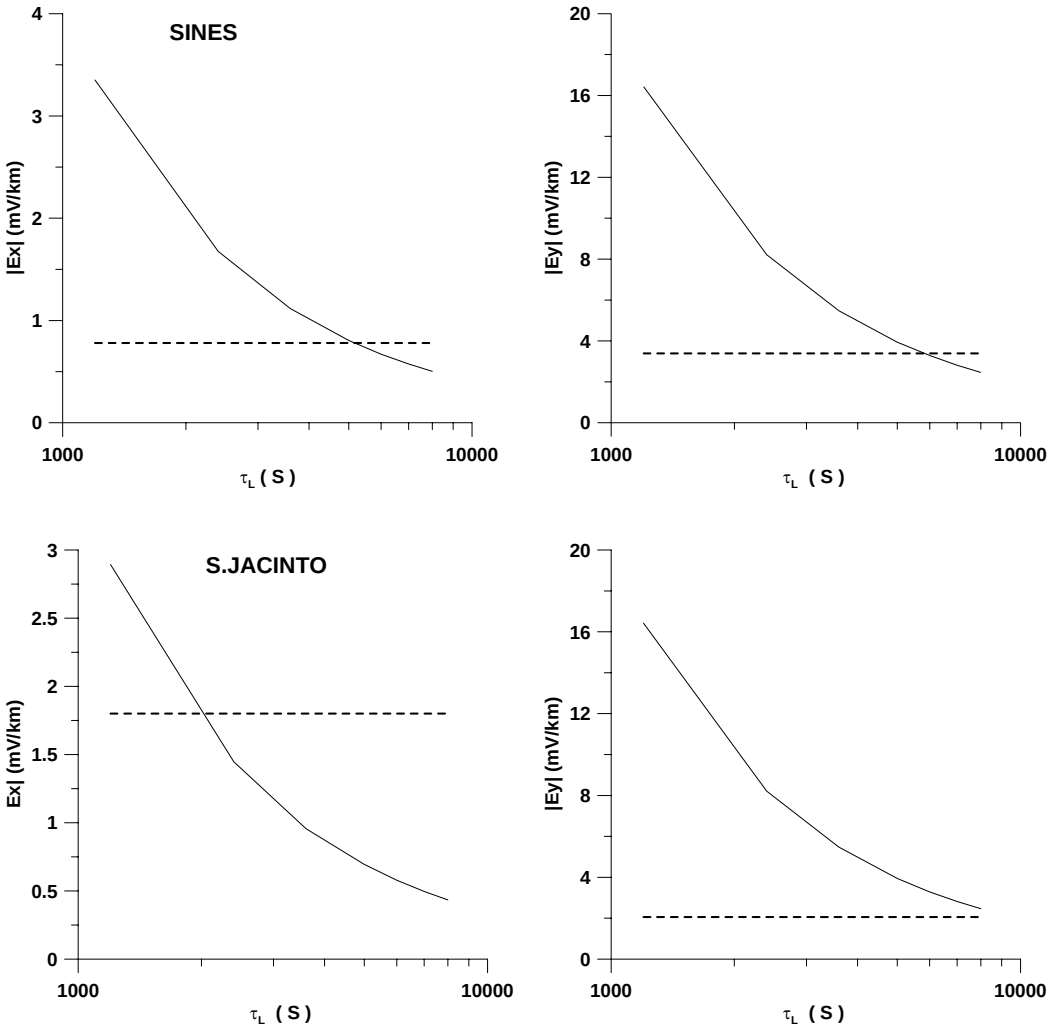

Figure 24. Predicted maximum amplitudes (solid lines) as a functions of $\log(\tau_L)$ and observed amplitudes (dashed straight lines) of M_2 tide electric field in Sines and São Jacinto. Calculations carried out assuming $h_w = 100$ m.

These results show that the on shore measurements mostly reflect the effect of the water transport in the direction N-S. The same result, e.g., the major importance of the E-W electric component is obtained considering a 200 m deep ocean. Since the electric field components are proportional to I_o / τ_L the earth conductance will the double of that one considered for a 100 m depth sea.

Conclusion

Electric fields data have been acquired in a submarine cable crossing a channel (the Barra in Aveiro area, northern Portugal) and in two onshore sites installed in the vicinity of the west Portuguese coastline and processed for tidal analysis. The main flows at the Barra channel have tidal origin and represent a key process in the water renewal at Ria de Aveiro lagoon.

It was shown that the dominant tidal component (period) in the submarine cable and onshore antennas data is the semidiurnal lunar period of 12.4602 h (the well known M_2 component). The data analysis reveals that measuring the differences of electric potential across the channel can provide an accurate estimate of the water transport by tidal flows through the Barra channel. A value of 720 $m^3\ s^{-1}\ mV^{-1}$ was estimated for the coefficient relating voltage and water transport at Barra.

It was also demonstrated that one can use the onshore lunar harmonics to estimate the water transport verified through the Barra channel. To achieve this, the onshore N-S antenna installed close to the Barra was calibrated by correlating the water transport tidal lunar and the onshore motionally tidal electric field. A calibration factor of 7350 m^3 s−1 for each mV/km, with motionally induced origin, was estimated for the N–S onshore dipole.

Onshore measurements of telluric field oscillations have been used to estimate the water transport associated to tidal flow in the western Portuguese coast. The onshore E-W dipoles located at São Jacinto and Sines were calibrated by correlating the N-S shelf water transport originated by the main lunar tidal frequency and the corresponding onshore motionally tidal electric field. Calibration factors of 3.00×10^4 and 4.25×10^3 $m^3\ s^{-1}$ for each mV km^{-1}, with motionally induced origin, was estimated for São Jacinto and Sines, respectively.

The possibility of using MIV methods to estimate flow transport on a short scale (about half of km) corresponding to estuarine systems and alongonshore, provides an important advantage over traditional oceanographic methods (classical currentmeter, Acoustic Doppler Currentmeter Profiler, ADCP, etc.). In this kind of environment the use of traditional methodologies is clearly limited in cost and in time, due to batteries and memory limitations, as well as to the very fast growth of algae that will make difficult the proper functioning of the instruments. Furthermore, concerning the water flow is usually determined from discrete measurements while when using ADCP's there are shadow areas close to both the bottom and to the surface, and therefore the obtained results are only approximate values. The MIV methods present low cost for accurate long-term monitoring of integral water transport.

Acknowledgments

This study was developed in the scope of the projects PROTEU (PDCTM/MAR/15275/1999) EMNOCM (POCTI/CTA/44062/2002) and AMDRAPHYD (POCI/AMB/57928/2004) funded by Fundação para a Ciência e Tecnologia (FCT) and by FEDER. One of the authors, R.N., was funded by a grant of the FCT (PRAXIS SFRH/BPD/10256/2002). The authors thank the Administration of the Port of Aveiro, Irmãos Cavaco, Xavisub and Área Militar de S. Jacinto for all aid along the equipment installation and data collection.

References

Chave, A.; Luther, D. Low-frequency, motionally induced electromagnetic fields in the ocean. *J. Geophys. Res*. 1990, 95, 7185–7200.

Dias, J.M., 2001. *Contribution to the Study of the Ria de Aveiro Hydrodynamics*, *PhD thesis,* Univ. de Aveiro, Portugal.

Dias, J.M.; Lopes, J. F. Implementation and assessment of hydrodynamic, salt and heat transport models: the case of Ria de Aveiro Lagoon). Portugal. *Environ. Model. Softw.* 2006, 21, 1–15.

Dias, J.M.; Lopes, J. F., Dekeyser, I. A numerical model system application to the study of the transport properties in Ria de Aveiro lagoon. *Ocean Dyn*. 2003, 53, 220–231.

Duffus, H. J.; Fowler N. R. On planetary voltages, ocean tides, and electric conductivity below the Pacific. *Can. J. Earth Sci*.1974, 11, 873-892.

Egedal, J. On the lunar-diurnal variation in the earth-currents. *Terr. Magn*. 1937, 42, 179–181.

Erofeeva, S.; Egbert, G. Efficient inverse modeling of barotropic ocean tides. *J. Oceanic Atmosph. Technol*. 2002, 19,183-204.

Filloux, J.H. 1987. Instrumentation and experimental methods for oceanic studies, *New Volumes in Geomagnetism*; 1, Academic, New-York, 143– 246.

Flosadottir, A. H.; Taire, K. *Proceedings of International Workshop on Scientific Use of Submarine Cables 1997*, 10–15. Observations of ocean currents using submarine cables.

Fristedt, T.; Sigray, P., Lundberg, P., Crona, L. Salt-wedge observations in Oresund by direct measurement of the motionally induced voltage. *Cont. Shelf Res*. 2002, 22, 2513–2524.

Fujii, I.; Utada, H. On geoelectric potential variations over a planetary scale. *Mem Kakioka Magn. Obs*. 2000, 29, 1-71.

Harvey, R. R.; Larsen, J. C. and Montaner. R. Electric field recording of tidal currents in the Strait of Magellan. *J. Geophys. Res*. 1977, 82, 3472-3476.

Junge, A. The telluric field in northern Germany induced by tidal motion in the North Sea. *Geophys. J. Int*. 1988, 95, 523–533.

Junge, A. and ISO-3D team Final Report of the ISO-3D project 2001, pp. 101–116: *Oscillations of the onshore telluric field generated by oceanic tides.*

Lanzerotti, L.J., Sayres, C. H., Medford, L.V., Kraus, J. S., and Maclennan, C. Earth potential over 4000 km between Hawaii and California. *J. Geophys. Res. Lett.* 1992, 19, 1177-1180.

Larsen, J.C. Florida Current volume transport from voltage measurements. *Science* 1985, 227, 292–311.

Larsen, J. C. Electric and magnetic fields induced by deep sea tides. *Geophys. J. Int.* 1968, *16*, 40–70.

Larsen, J. C. The electromagnetic field of long and intermediate water waves. *J. Mar. Res.* 1971, *29* (1), 28–45.

Larsen, J. C. Transport and heat flux of the Florida Current at 27 N derived from cross-stream voltages and profiling data: Theory and observations. *Phil. Trans. R. Soc. Lond*. 1992*,* A, 338, 169–236.

Longuet-Higgens, M. S. The electric and magnetic effects of tidal streams. *Mon. Not. Roy. Astr. Soc. (Geophys. Suppl.)* 1949, 5, 285–307.

Malin, S. R. C. Separation of lunar daily variations into parts of ionospheric and oceanic origin. *Geophys. J. R. Astron. Soc*. 1970, 21, 447–455.

Marques, C. A. F.; Ferreira, J. A., Rocha, A., Castanheira, J. M., Melo-Goncalves, P., Vaz, N. and Dias, J. M. Singular spectrum analysis and forecasting of hydrological time series. *Phys. Chem. Earth* 2006, 31, 1172–1179.

Marta-Almeida, M.; Dubert, J. The structure of tides in the Western Iberian region. *Cont. Shelf Res*. 2006, 26, 385–400.

Marta-Almeida, M.; Dubert, J., Peliz, A., dos Santos, A. and Queiroga, H. A modelling study of the Norway Lobster (Nephrops norvegicus) larval dispersal in southern Portugal: predictions of larval wastage and self-recruitment in the Algarve stock. *Can*. J. *Fish. Aquat. Sci*. 2008, 65, 2253–2268.

Marta-Almeida, M., Monteiro Santos, F.A., Nolasco, R., Dubert, J., Bernardo, I., Soares, A., Peliz, A. and Dias, J., 2010. On the estimation of tidal and subinertial alongshore water transport from onshore telluric measurements. *Physics of the Earth and Planetary Interior* (submitted).

Maus, S.; Kuvshinov, A. Ocean tidal signals in observatory and satellite magnetic measurements. *Geophys. Res. Lett*. 2004, 31, doi: 10.1029/2004GL000634.

McKnight, J. D. Lunar daily variations in New Zealand. *Geophys. J. Int*. 1995, 122, 889–898.

Monteiro Santos, F. A.; Nolasco, R., Soares, A., Dias, J. and Bernardo, I. Estimation of water transport from oscillations of the onshore telluric field generated by tides. *Earth Planet.* Sc. Lett. 2007, 263, 420–428.

Monteiro Santos, F. A.; Soares, A., Trindade, L., Nolasco, R. and Rodrigues, H. Voltage measurements over the CAM-1 submarine cable between Madeira Island and Portugal mainland. *Earth Planets Space* 2002, 54, 393–398.

Nolasco, R.; Soares, A., Dias, J. M., Monteiro Santos, F. A., Palshin, N. A., Represas, P. and Vaz, N. Motional induction voltage measurements in estuarine environments: the Ria de Aveiro Lagoon (Portugal). *Geophys. J. Int*. 2006, 166, 126–134.

Palshin, N. A.; Vanyan, L. L., Kaikkonen P. Onshore amplification of the electric field induced by a coastal sea current. *Physics of the Earth and Planetary Interiors* 1996, 94, 3-4, 269-273.

Palshin, N. A.; Vanyan, L. L., Medzhitov, R. D., Shapiro, G. I., Evdoshenko, M. A., Utada, H., Shimizu, H. and Tanaka, Y. Use of the Nakhodka-Naoetsu submarine cable for studying the temporal variability of the integral water transport in the Sea of Japan. *Oceanology* 2001, 41, 447–453.

Palshin, N. A.; Vanyan, L., Yegorov I., Lebedev, K. Electric field induced by the global ocean circulation. *Physics Solid Earth* 1999, 35, 1028-1035.

Palshin, N. A.; Vanyan, L.L., Poray-Koshits, A.M., Matyushenko, V.A., Kaikkonen, P., Tiikkainen, J. Measurements of motionally induced voltage in the coastal zone of the Throat of the White Sea. *Earth Planets Space* 2002, 54, 433–441.

Pawlowicz, R.; Beardsley, B. and Lentz, S. Classical tidal harmonic analysis including error estimates in MATLAB using T TIDE. *Comput. Geosci*. 2002, 28, 929–937.

Peliz, A.; Dubert, J., Marchesiello, P. and Teles-Machado, A. Surface circulation in the Gulf of Cadiz: Model and mean flow structure. *J. Geophys. Res*. 2007a, 107, C11 015.

Peliz, A., P. Marchesiello, A. M. P. Santos, J. Dubert, A. Teles-Machado, M.Marta-Almeida, and B. Le Cann, 2009: Surface circulation in the Gulf of Cadiz: 2. Inflow-outflow coupling and the Gulf of Cadiz slope current. *J. Geophys. Res*., 114, C03 011.

Penven, P.; Debreu, L., Marchesiello, P. and McWilliams, J. C. Evaluation and application of the ROMS 1-way embedding procedure to the central california upwelling system. *Ocean. Model*. 2006, 12, 157–187.

Rooney, W.J. Lunar diurnal variation in Earth currents at Huancayo and Tuscon. *J. Geophys. Res*. 1938, 43, 107-118.

Sanford, TMotionally-induced electric and magnetic fields in the sea. . *J. Geophys. Res*. 1971, 76, 3476–3492.

Shchepetkin, A. F.; McWilliams, J. C. A method for computing horizontal pressure-gradient force in an oceanic model with a non-aligned vertical coordinate. *J. Geophys. Res*. 2003, 108, 1–34.

Shchepetkin, A. F.; McWilliams, J. C. The Regional Ocean Modeling System (ROMS): A splitexplicit, free-surface, topography-following coordinates ocean model. *Ocean. Model.* 2005, 9, 347–404.

Skamarock, W. C.; Klemp, J. B., Dudhia, J., Gill, D. O., Barker, D. M., Wang, W. and Powers, J. G. Tech. rep., MMMD-NCAR, Boulder, Colorado, USA. 2005. *A description of the Advanced Research WRF Version 2.*

Szuts, Z., 2008. *The interpretation of motionally induced electric fields in oceans of complex geometry.* PhD Thesis, University of Washigton, 190 p.

Teles-Machado, A.; Peliz, A., Dubert, J., and Sanchez, R. On the onset of the Gulf of Cadiz Coastal Contercurrent. *Geophys. Res. Lett*. 2007, 34.

Tyler, R.; Mysak, L. A., and Oberhuber, J. Electromagnetic fields generated by a 3-D global ocean circulation. *J. Geophys. Res*. 1997, 102, 5531-5551.

Tyler, R.; Maus, S. and Luhr, H. Satellite observations of magnetic fields due to ocean tidal flow. *Science* 2003, 299, 239–241.

Tyler, R.; Oberhuber, J. and Sanford T. The potential for using ocean generated electromagnetic field to remotely sense ocean variability. *Phys. Chem. Earth A* 1999, 24, 429– 432.